Seismic attenuation in fractured porous media: insights from a hybrid numerical and analytical model

Seismic attenuation in fractured porous media: insights from a hybrid numerical and analytical model

Ekanem, A. M.[1, 2, 3]; Li, X. Y.[3, 4], Chapman, M.[2, 3] and Main, 1.G.[2]

*[1] Department of Physics, Akwa Ibom State University, Mkpat Enin, Nigeria (**current address**)*
[2] School of Geosciences, University of Edinburgh, EH9 3JW, United Kingdom
[3] British Geological Survey, Murchison House, Edinburgh, EH9 3LA, United Kingdom
[4] CNPC Geophysical Key Laboratory, China University of Petroleum, Beijing, China

Abstract

Seismic attenuation in fluidsaturated porous rocks can occur by geometric spreading, wave scattering or the internal dissipation of energy, most likely due to the 'squirt-flow' mechanism. In principle the pattern of seismic attenuation recorded on an array of sensors then contains information about the medium, in terms of material heterogeneity and anisotropy, as well as material properties such as porosity, crack density and pore-fluid composition and mobility. In practice this inverse problem is challenging. Here we provide some insight into the effect of internal dissipation from analysing synthetic data produced by a hybrid numerical and analytical model for wave propagation in a fractured medium embedded in a layered geological structure. The model is made up of one anisotropic and three isotropic horizontal layers. The anisotropic layer consists of a porous, fluid-saturated material containing vertically-aligned inclusions representing a set of fractures. This combination allows squirt-flow to occur between the pores in the matrix and the model fractures. . Our results show that the fluid mobility, and the associated relaxation time of the fluid-pressure gradient controls the frequency range over which attenuation occurs. The induced attenuation increases with incidence angle and azimuth away from the fracture strike direction. Azimuthal variations in the induced attenuation are elliptical, allowing the fracture orientations to be obtained from the axes of the ellipse. These observations hold out the potential of using seismic attenuation as an additional diagnostic in the characterisation of rock formations for a variety of applications, including hydrocarbon exploration and production, subsurface storage of CO2 or geothermal energy extraction.

Keywords: Attenuation, Anisotropy, Seismic Quality Factor, Fluid Mobility, Squirt Flow

1.0 Introduction

The propagation of seismic wave through a given medium causes slight deformation in the medium which generates local stress and strains. If the medium is saturated with a fluid and is also porous, local gradients in deformation will arise due to micro-structural disorder in the material, in turndriving fluid movement: between different parts of the same pore, between connected pores of different sizes, and between pores and fractures. This mechanism is known as 'squirt flow', and results in to anelastic seismic attenuation by viscous dissipation (Chapman, 2003). Equivalent medium theories for this process (e.g. Tod, 2001; Chapman, 2003) predict azimuthal variations in the induced attenuation for seismic wave propagation in a medium with a set of aligned fractures. Indeed, azimuthal variations in P-wave attenuation have been observed in both laboratory and field data (e.g. Clark *et al.,* 2001; Luo *et al.,* 2006; Chichinina, *et al.,* 2006; Maultzsch *et al*., 2007; Clark *et al*., 2009, Ekanem *et al.*, 2013, Ekanem *et al.*, 2014) and has been linked to fracture properties. Attenuation has been observed to have higher magnitudes in fluid-saturated rocks than in dry rocks (e.g. Gardner *et al* 1964, Toksöz *et al*., 1979, Johnston and Toksöz 1980, Johnson 1981, Winkler 1986). The squirt-flow mechanism results in dispersion as well as attenuation, as described in the model of (Chapman, 2003). In this theoretical model the time needed to relax the pressure (relaxation time) is dependent on fluid mobility, defined as the ratio of permeability to viscosity. High fluid mobility enhances pore-pressure equilibrium, resulting in low-frequency domain where Gassmann's equations are valid, while lower fluid mobility requires more time to equilibrate pore-pressure (Batzle *et al*., 2006). Thus, an inverse relationship exists between fluid mobility and relaxation time.

Batzle *et al.* (2006) examined the influence of fluid mobility on seismic velocity dispersion in laboratory measurements from seismic to ultrasonic frequencies. Their broad-band measurements demonstrate that velocity dispersion can be significant, and is strongly influenced by fluid mobility. Ekanem *et al.* (2013) examined the effect of attenuation anisotropy in laboratory scale model meant to study the effects of dry cracks and found that P-wave attenuation exhibits anisotropic characteristics which could be linked with the fracture properties. Despite intensive effort in research and development, the task of using P-wave attenuation attribute for fracture prediction in the Earth's crust still needs more understanding of the underlying principle. A concerted effort is needed to get more insight of attenuation characteristics in fractured porous media using theoretical models to aid our understanding of the underlying physics even as this attribute continues to gain popularity as a useful tool in hydrocarbon exploration. This is especially of high value to reduce risks in exploration.

In this paper, we have carried out a numerical modelling study of P-wave attenuation characteristics in fractured porous media. A hypothetical medium is constructed to represent a fractured porous formation embedded in a layered geological structure. The properties of the fractured layer are chosen to allow squirt-flow to occur, and the seismic response is calculated using Chapman's (2003) mean-field equivalent medium theory. The mean field theory does not account for multiple scattering. The material properties of all of the layers are assigned values that are representative of real field cases. The seismic response of the medium at different positions on the surface of the first layer is then calculated numerically. Maultzsch *et al.* (2007) previously used this approach to investigate the effects of attenuation anisotropy using a walk-away VSP geometry, and observed anisotropic attenuation which has an elliptical variation with azimuth. We extend their study to the case of surface seismic geometry to gain a more complete understanding of the anisotropic characteristics. Firstly, we examine the influence of fluid mobility on the induced attenuation and then its anisotropic behavior. We used the classical spectral ratio method to compute the induced attenuation for selected offsets from the synthetic data. The results of our study show that the fluid-pressure gradient's relaxation time (or the inverse of fluid mobility) strongly controls the frequency range over which attenuation occurs. The induced attenuation increases in magnitude with incidence (polar) angle (offset) and away from the fracture strike direction. Azimuthal variations in the induced attenuation are elliptical and the fracture orientations are obtained from the axes of the ellipse. The results provide significant new insight into the causes and effects of the pattern of seismic attenuation in fractured-porous rocks, and hold out the potential of using seismic attenuation as an additional diagnostic in the characterisation of rock formations for a variety of applications, including hydrocarbon exploration and production, subsurface storage of CO2 or geothermal energy extraction.

1.1 Chapman's poro-elastic model

The poro-elastic model of Chapman (2003) considers the pore space of a rock to consist of a lattice configuration of spherical pores, randomly oriented ellipsoidal micro-cracks and aligned ellipsoidal fractures. The radius of the micro-cracks and spherical pores is identified with the grain size. The fracture size is much larger than the grain size but smaller than the seismic wavelength. Since the fractures have preferential alignment, the resulting medium has hexagonal symmetry (transverse isotropy). Wave-induced pressure gradients cause fluid exchange between adjacent elements of pore space in the rock. The fluid exchange between two adjacent voids 'a' and 'b' for instance is described by the formula (Chapman 2003):

$$\partial_t m_a = \frac{\rho_o \kappa \varsigma}{\eta}\left(p_b - p_a\right) \tag{1}$$

where ρ_o is the fluid density, κ is the permeability, ς is the grain size, η is the fluid viscosity, p_a is the pressure in element a, m_a is the mass of fluid in element a and p_b is the pressure in element b. Each element of pore space is assumed to be connected to six other elements and the resulting flows can be added linearly. The fractures are connected to a greater number of elements since they are larger than the micro-cracks and the pores. For the purpose of ensuring that there is some spacing between the fractures, the model assumes that each micro-crack or pore is connected to at most one fracture and that the fractures are not connected to each other. These last assumptions require that the number of micro-cracks and pores greatly exceeds the number of fractures. The effective elastic tensor, C given by Chapman (2003) is of the form:

$$\mathbf{C} = \mathbf{C}^{(0)} - \phi_p \mathbf{C}^{(1)} - \varepsilon_c \mathbf{C}^{(2)} - \varepsilon_f \mathbf{C}^{(3)} \tag{2}$$

where $C^{(0)}$ is the elastic tensor of the isotropic rock matrix with Lame's parameters λ and μ, $C^{(1)}$, $C^{(2)}$ and $C^{(3)}$ are the additional contributions from pores, micro-cracks and fractures, respectively, multiplied by the porosity ϕ_p, the crack density ε_c and the fracture density ε_f. These additional contributions are functions of the Lamé parameters, fluid and fracture properties, frequency and relaxation times associated with squirt flow.

Chapman's (2003) original model is restricted to very low porosity since the elastic constants are calculated based on Eshelby's (1957) interaction energy approach which is only valid for dilute concentrations of inclusions (Maultzsch *et al.*, 2003). In cases of high porosities, the calculation of the corrections using the grain moduli λ and μ might result in significant errors. Furthermore, it is not ideal to use moduli which cannot be obtained from measured velocities. To address these issues, Chapman *et al.* (2003) slightly adapted the model to make it more applicable to real data by using Lame's parameters λ^o and μ^o derived from the density ρ and measured P-wave velocity V_p^o and S-wave velocity V_s^o of the un-fractured rock for the corrections. Also, $C^{(0)}(\Lambda, M)$ is defined in such a way that the measured isotropic velocities are obtained by applying the pore and crack corrections at a specific frequency f_o (Chapman *et al.,* 2003 and Maultzsch *et al*., 2003). Thus:

$$\Lambda = \lambda^{o} + \phi_{c,p}\left(\lambda^{o},\mu^{o},f_{o}\right), \quad M = \mu^{o} + \phi_{c,p}\left(\lambda^{o},\mu^{o},f_{o}\right), \tag{3}$$

where $\phi_{c,p}$ refers to corrections to the elastic tensor which are proportional to crack density and porosity.

$$\lambda^{o} = \rho\left(V_{p}^{o}\right)^{2} - 2\mu^{o}\ ; \quad \mu^{o} = \rho\left(V_{s}^{o}\right)^{2} \tag{4}$$

Equation 2 can then be re-written as:

$$C = C^{(0)}(\Lambda, M, \omega) - \phi_{p}C^{(1)}\left(\lambda^{o}, \mu^{o}, \omega\right) - \varepsilon_{c}C^{(2)}\left(\lambda^{o}, \mu^{o}, \omega\right) - \varepsilon_{f}C^{(3)}\left(\lambda^{o}, \mu^{o}, \omega\right) \tag{5}$$

The form of Equation 5 allows the corrections for pores, micro-cracks and fractures which describe the frequency dependence and anisotropy of a material to be obtained from measurements of the velocities (Maultzsch *et al*., 2003). Chapman *et al.* (2003) further simplified the model by setting the crack density to zero in the case of high porosity. The influence of this parameter however is not significant for modelling the effects of fractures provided the spherical porosity is much greater than the crack porosity (Maultzsch *et al*., 2003).

Fluid flow in Chapman's (2003) model occurs at two scales; the grain scale (associated with the micro-cracks and spherical pores) and the fracture scale. This results in two characteristic frequencies and corresponding relaxation times. The relaxation time, τ_{m} associated with fluid flow between the micro-cracks and spherical pores are related to the squirt-flow frequency, f_{m}^{c} as (Murphy, 1985; Winkler, 1986; Lucet and Zinszner, 1992; Sothcott *et al*., 2000):

$$f_{m}^{c} = \frac{1}{\tau_{m}} \tag{6}$$

$$\tau_{m} = \frac{c_{v}\eta\left(1 + K_{c}\right)}{\sigma_{c}\kappa\varsigma_{1}}, \tag{7}$$

where c_v is the volume of an individual crack, σ_{c} is the critical stress and c_1 is the number of connections to other voids. σ_{c} and K_c are defined by:

$$\sigma_{c} = \frac{\pi\mu\, r}{2\left(1 - \nu\right)} \tag{8}$$

$$K_{c} = \frac{\sigma_{c}}{\kappa_{f}} \tag{9}$$

where *r* is the aspect ratio of the cracks, *v* is the poison's ratio of the matrix and κ_f is the fluid bulk modulus. Fluid flow in and out of the fractures is associated with a lower characteristic frequency or a higher corresponding relaxation time τ_f which is dependent on the size of the fractures. The relaxation time associated with the grain scale and that associated with the fracture scale are both related by the equation (Chapman, 2003):

$$t_f = \frac{a_f}{\varsigma}\tau_m \tag{10}$$

where a_f is the fracture radius. From Equation 10, it can be inferred that larger fractures will result in higher relaxation times (or lower characteristic frequencies). These larger relaxation times lead to velocity dispersion and attenuation in the seismic frequency range. Thus, the resulting anisotropy is frequency dependent.

1.2 Fluid mobility

Fluid mobility (m_f) defined as the ratio of permeability to viscosity (Equation 11) is found to greatly influence the propagation of seismic wave (Batzle *et al.,* 2006).

$$m_f = \frac{k}{\eta} \tag{11}$$

The propagation of seismic wave through a given medium results in slight deformation in the medium which generates stress and strains. If the medium is saturated with a fluid and also porous, the stress generated is just sufficient to cause fluid movement (mobility). The time needed to equalize the pressure difference (relaxation time) depends on fluid mobility. High fluid mobility enhances pore-pressure equilibrium, resulting in a low frequency domain where Gassmann's equations are valid whereas low fluid mobility implies that the pore-pressure remains out of equilibrium, resulting in the high frequency domain (Batzle *et al.,* 2006). Most rocks in the sedimentary basin (e.g. shales, siltstones, tight limestones) have low permeability and mobility and thus, are in the high frequency domain even at seismic frequencies (Batzle *et al.,* 2006). In between these two frequency domains is the transition frequency band where seismic anisotropy is frequency-dependent and could be used to deduce fracture and fluid properties (Qian *et al.*, 2007).

An inverse relationship exists between fluid mobility and relaxation time as implied in Equation 7 (other parameters remaining constant). Higher fluid mobility implies lower

relaxation time and vice versa. Since fluid movement causes attenuation, it follows therefore that changes in the relaxation times could lead to changes in the fluid mobility and hence, the induced attenuation. At what relaxation time is the attenuation maximum or minimum and where lies the transition between the two limiting cases? Thus, we first investigate the effects of fluid mobility on the induced P-wave attenuation by considering a range of values of relaxation times in Chapman's (2003) poro-elastic model. We subsequently use the value at maximum attenuation to investigate the anisotropic characteristics of the induced attenuation.

2.0 The hypothetical medium The hypothetical medium is made up of one anisotropic and three isotropic horizontal layers. The anisotropic layer (third layer) consists of a porous fluid-saturated material with aligned vertical fractures, allowing squirt flow between the pores in the matrix and the fractures. The elastic properties of the material are calculated analytically using the mean-field poro-elastic model of Chapman (2003). Details of the model parameters are given in Table 1.

Table 1: Model parameters

(a) Layer parameters

Layer	v_p (m/s)	v_s (m/s)	ρ (Kg/m^3)	Thickness (m)
1	1500	1000	1000	400
2	2314	1100	1150	600
3	2610	1300	1750	600
4	3100	1800	2200	Half space

(b) Fracture model parameters

Porosity	0.08
Crack density	0
Fracture density	0.1
Fracture radius	10 cm
Fluid bulk modulus	2.0Gpa
Frequency	50 Hz
Grain size	200 μm

The synthetic data for this model were computed from the theoretical model using the 'Aniseis' software (Taylor 2001) which makes use of the reflectivity method. A Ricker wavelet with a centre frequency of 25 Hz and a start time of 100 ms was used as the source wavelet. The source is an explosive source and was placed on the surface of the model. The software modifies the explosive source such that outward waves are suppressed and only contributions from waves directed into the model are generated (Taylor, 2001). The resulting

wavefield was calculated at some 21 positions at the surface of layer 1, at a regular spacing of 200 m, and a source - receiver spacing of 200 m was maintained. The synthetic ata were recorded with a time step of 1 ms and a total sampling time of 3 s.

To investigate the effect of fluid mobility on the induced P-wave attenuation, we used values of relaxation times ranging from $2x10^{-8}$ to $2x10^{-3}$ s in Chapman's (2003) poro-elastic model to compute the synthetic data in a direction perpendicular to the fracture strike direction. These relaxation times are associated with fluid flow at the grain scale. We then used the relaxation time value at maximum attenuation to investigate the anisotropic characteristics of the induced attenuation by computing synthetic data at four azimuths (0°, 45°, 60° and 90°) relative to the fracture strike direction. 0° azimuth corresponds to the fracture strike direction while 90° azimuth corresponds to the fracture normal direction. Seismic physical modelling studies by Ekanem *et al*. (2013) have shown that for dry fractures, attenuation is minimum and maximum in these directions respectively. Sample synthetic data are shown in Figure 1,. The data are consistent with the pattern of arrivals expected from the geometry of the assumed geological model and the absence of multiple scattering in the mean field model (simple wavelets without an extended complex coda)

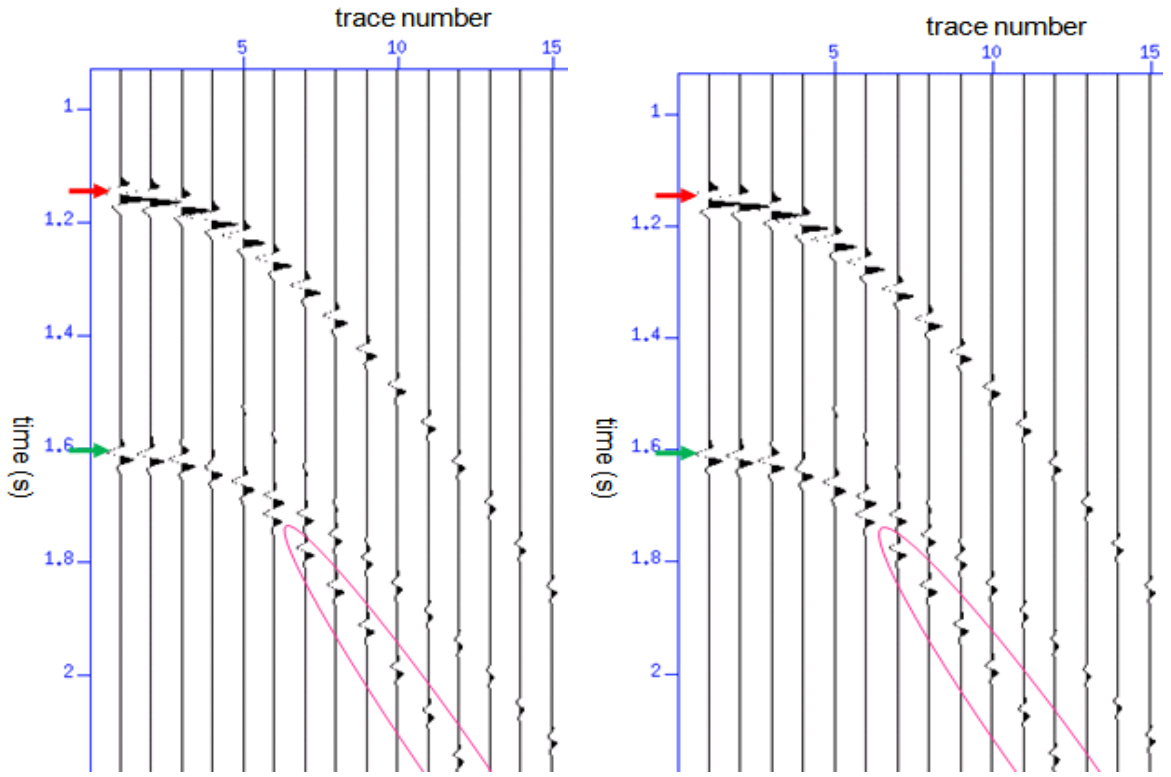

(a) (b)

Figure 1: Sample synthetic gathers (a) relaxation time (Tau0) = $2x10^{-8}$ s (b) relaxation time (Tau0) = $2x10^{-5}$ s. The red and green arrows indicate the top and bottom fractured-layer

reflections respectively while the pink colour highlights the converted wave. The trace spacing is 200 m.

3.0 Attenuation measurement

Attenuation is usually expressed as the inverse of the seismic quality factor, Q. Among the various methods of estimating Q from seismic data, the spectral ratio method is very common perhaps because of its ease of use and stability (e.g. Hauge 1981; Pujol and Smithson 1991; Dasgupta and Clark 1998), and because it removes the effects of geometric spreading in a simple way. Thus any measurement of attenuation can be attributed solely to internal energy dissipation or 'intrinsic attenuation'. In this study, we used the spectral ratio method to estimate the seismic quality factor from the synthetic data for selected offsets. In each gather, the first trace from the top model reflection at an offset of 0 m was used as the reference trace for comparison of the spectral ratios. The power spectra of the reflection events from the top and bottom of the fractured-layer and their ratios to that of the reference event were computed according to Equation 12. We used a constant time window of 140 ms for these events and computed the power spectra using the FFT algorithm.

$$\ln \frac{A_2^{\,2}}{A_1^{\,2}} = \ln \frac{P_2}{P_1} = 2\ln(RG) - \frac{2\pi f}{Q}(t_2 - t_1) \qquad (12)$$

f is frequency, R is the reflectivity term, G is the geometrical spreading factor, A_1 is the spectral amplitude of the reference trace, A_2 is the spectral amplitude of the target reflection (top or bottom of fractured-layer) while P_1 and P_2 are the respective spectral powers (square of amplitudes), t_1 and t_2 are the corresponding travel times, Q is the seismic quality factor down to the reflector.

Figures 2 and 3 show sample Log Power Spectral Ratios (LPSR) - frequency plots for the relaxation times and four azimuths considered. The plots are approximately linear between the frequency bandwidth of 20 - 90 Hz. Next, we performed a simple least squares-regression of the Log of the Power Spectral Ratios against frequency according to Equation 12 using a constant frequency bandwidth of 20 - 90 Hz for all the traces analysed. Sample least-squares regression plots of the LPSR against frequency for the chosen bandwidth are shown in Figures 4 and 5 for the top and bottom fractured-layer reflections respectively with their corresponding R^2 values. The plots show good fit of the spectral ratios, indicating a linear

relationship as predicted by Equation (12) even though attenuation is frequency dependent in the model (Equation 10).

For a given offset, we computed Q down to the reflector from the slope, p of the least square regression given by:

$$p = -\frac{2\pi(t_2 - t_1)}{Q} \tag{13}$$

With the pair of Q values computed for the top and bottom of the fractured-layer, we used the layer-stripping method of Dasgupta and Clark (1998) to compute the interval Q_i value in the fractured layer using the equation:

$$Q_i = \frac{[t_2 - t_1]}{t_2/Q_2 - t_1/Q_1} \tag{14}$$

where Q_1 and Q_2 are the seismic quality factors down to top and bottom of the fractured-layer respectively.

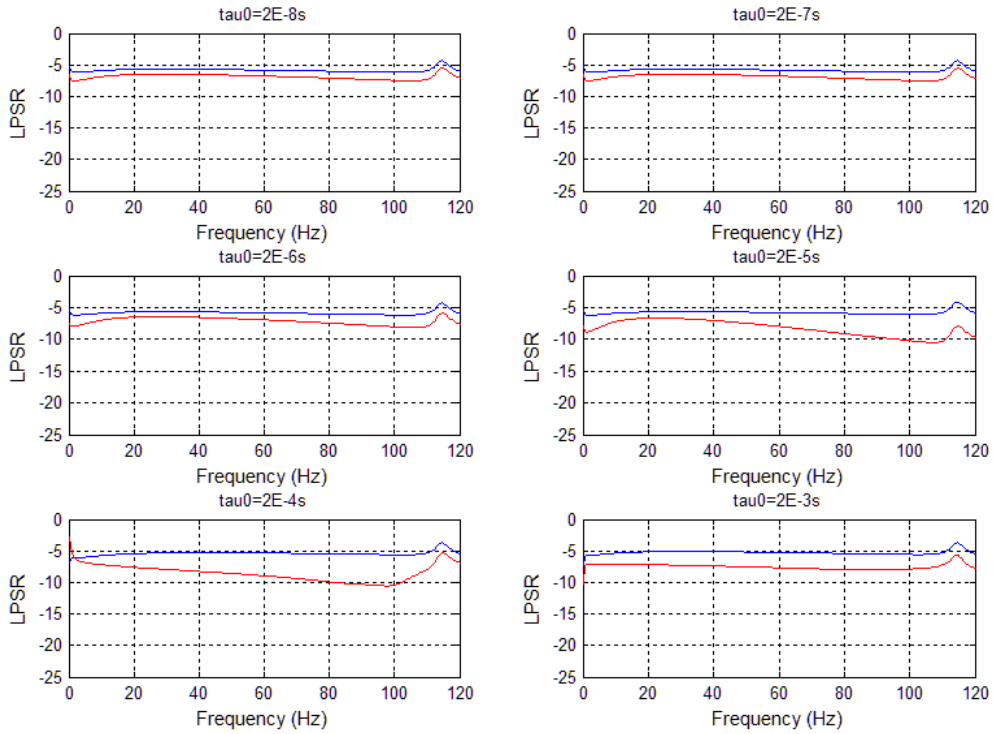

Figure 2: Log Power Spectral Ratio (LPSR) - frequency plots for the relaxations times (tau0) considered at a fixed offset of 1800 m. The blue and red lines indicate the top and bottom fractured-layer reflections respectively.

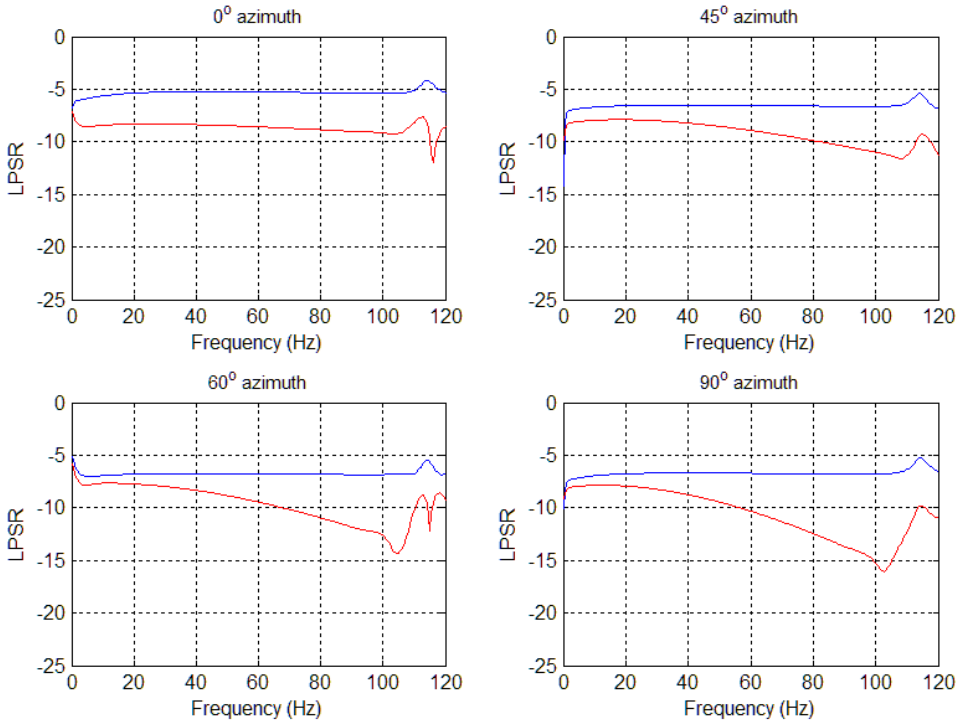

Figure 3: Log Power Spectral Ratio (LPSR) - frequency plots for the four azimuths considered at a fixed offset of 2600 m. The blue and red lines indicate the top and bottom fractured-layer reflections respectively.

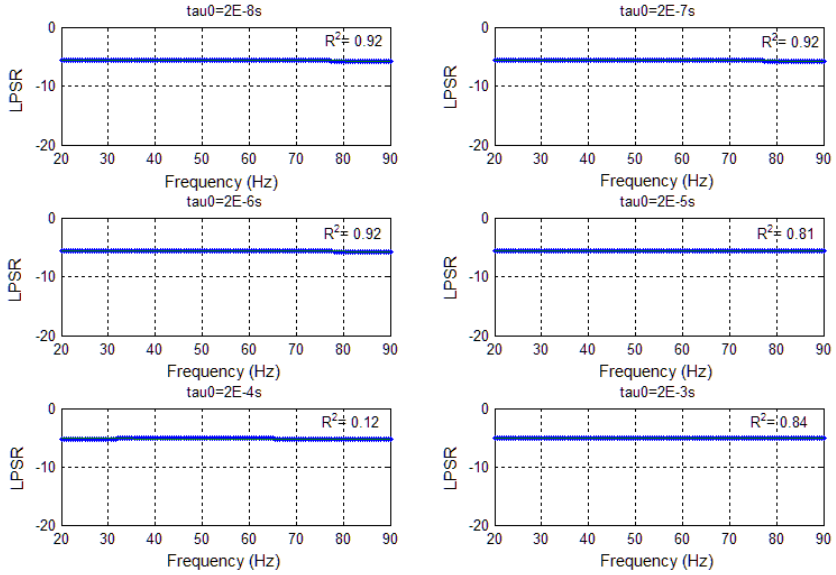

Figure 4: LPSR plots against frequency for the relaxation times (tau0) considered at a fixed offset of 1800 m for top fractured-layer reflection. The plots are approximately horizontal.

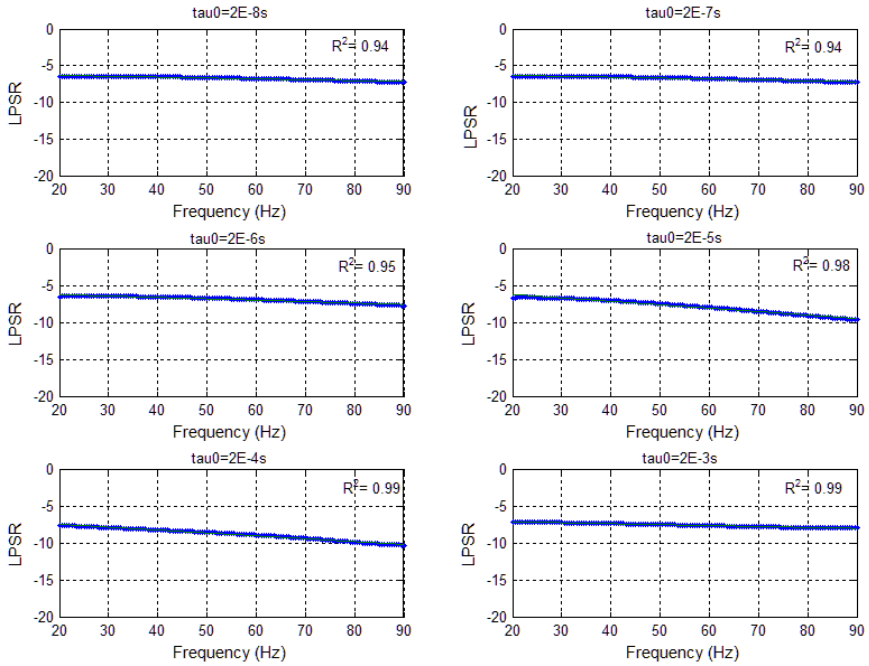

Figure 5: LPSR plots against frequency for the relaxation times (tau0) considered at a fixed offset of 1800 m for bottom fractured-layer reflection.

4.0 Results and discussion

The results of our study show that the induced P-wave attenuation is dependent on the relaxation time and hence fluid mobility (Figure 6). Lower attenuation values (1/Q) are obtained at relaxation times $\leq 2x10^{-6}$s (or relaxation frequency $\geq$ 500 KHz) and $\geq 2x10^{-3}$s (relaxation frequency $\leq$ 500 Hz) respectively. However, higher attenuation values are obtained between relaxation times of $2x10^{-6}$ s to $2x10^{-3}$ s with maximum attenuation at a relaxation time of around $2x10^{-5}$s (or relaxation frequency of 50 kHz). These relaxation times and corresponding frequencies are associated with fluid flow at the grain scale. With fracture radius of 10 cm and grain size of 200 μm, the relaxation times at the fracture scale and the corresponding frequencies can be computed using Equation 10. The attenuation is assumed to occur because of the relaxation of the fluid-pressure gradients generated by the propagation of seismic waves between the fractures and the surrounding pore space. The time taken to relax the pressure gradient strongly controls the frequency range over which the attenuation occurs. High fluid mobility implies lower relaxation times and vice versa. Thus, fluid mobility divides the relaxation time into three zones; high relaxation time zone often regarded as the relaxed state, low relaxation time zone often regarded as the un-relaxed state and a transition between them (intermediate relaxation time zone) as shown in Figure 6. Higher relaxation times imply that more time is required to relax the pressure gradient generated by the propagation of P-waves in the rock and the pore pressure is therefore out of equilibrium resulting in the high frequency regime. Fluid mobility and hence the induced

attenuation is low in this regime and the model tends to Hudson's (1980) model of non-communicating cracks or fractures. On the other hand, lower relaxation times mean that less time is needed to relax the pressure gradient generated by wave propagation in the rock and the pore pressure equilibrium is enhanced resulting in the low frequency regime. Fluid mobility is high in this regime and Gassmann's relation is valid. In between these two zones, attenuation occurs with a maximum magnitude at a relaxation time of around $2x10^{-5}$s (or relaxation frequency of 50 kHz).

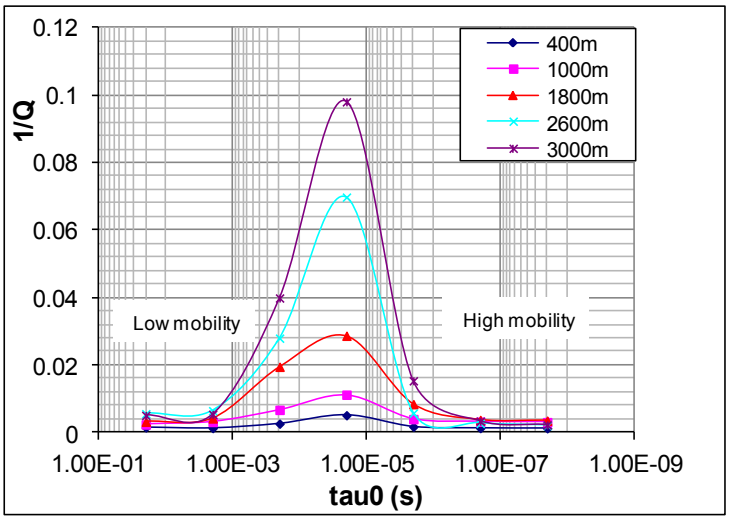

Figure 6: Attenuation (inverse quality factor 1/Q) computed for the field scale model as a function of relaxation times (tau0) for selected offsets provided in the key..

Our results also show that the induced attenuation varies both with incidence angle and azimuth relative to the fracture strike direction. Attenuation increases with incidence angle and also away from the fracture strike direction with maximum attenuation normal to the fractures (Figure 7) which is consistent with the results of the seismic physical modelling studies of Ekanem *et al*. (2013) and walk away VSP studies of Maultzsch *et al.,* (2007). Azimuthal variations in the attenuation are elliptical to a good approximation (Figure 8). These plots, which are analogous to slowness surfaces, are a convenient graphic representation of attenuation anisotropy. A minimum offset of 400 m (or 8.4° incidence angle) corresponding to an offset-depth ratio of 0.4 and 0.25 respectively to the top and bottom of the fractured-layer is required to reveal the anisotropy. The magnitude of the observed attenuation anisotropy increases with offset up to a maximum of 5.1 % at 3400 m offset. The major axis of the Q - ellipse corresponds to the fracture strike where attenuation is a minimum, while the minor axis corresponds to the fracture normal where attenuation is a maximum.

Further analysis of our results shows that the azimuthal variations in the induced attenuation obey a cosine fit of the form (Maultzsch *et al*. 2007):

$$\Delta Q^{-1} = C1 + C2\cos[2(\theta - \theta_o)] \tag{15}$$

where *C1* is an arbitrary constant, *C2* is the magnitude of azimuthal variation, θ is the azimuthal angle and θ_o is the fracture normal direction at which attenuation is maximum. Figure 9 shows the cosine fits to the Q results for selected offsets. The magnitude of the attenuation anisotropy increases with incidence angle or offset (Figure 10a). The azimuth of maximum attenuation from the cosine fit is 90° which corresponds to the fracture normal (Figure 10b). These results show a strikingly good agreement with the best-fitting ellipse..

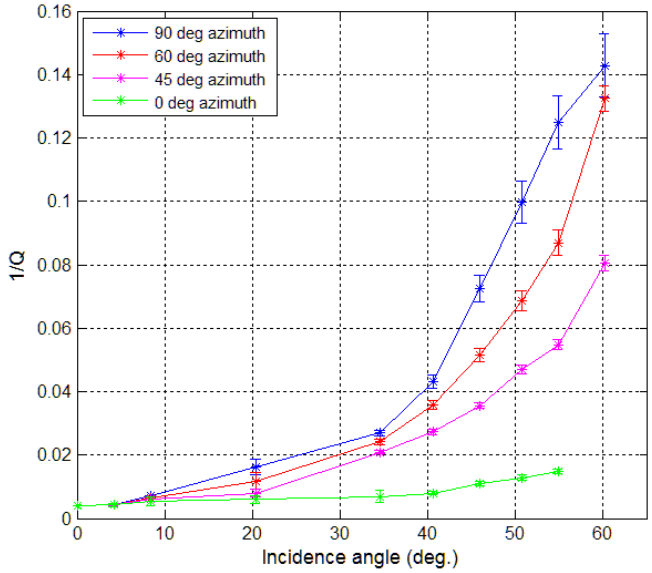

Figure 7: Q profile with incidence angles. Attenuation increases with incident angles. There is no significant change of attenuation with incidence angle at the fracture strike azimuth (0° azimuth).

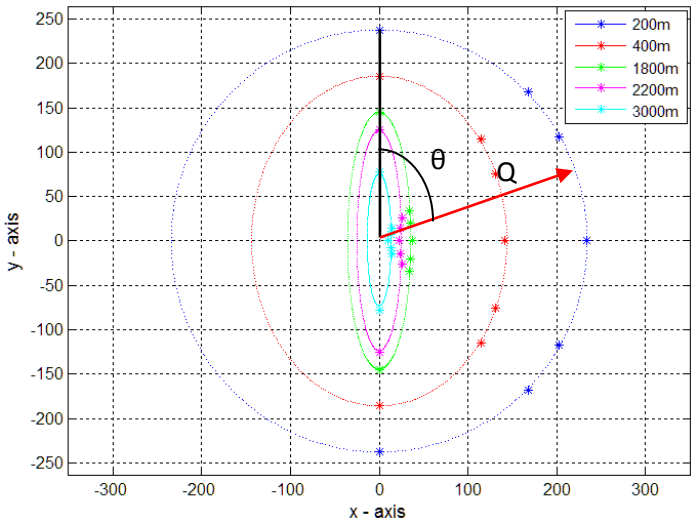

Figure 8: Q anisotropy ellipse. The ellipse has a centre at (0, 0) and the distance from the centre of the ellipse to the surface (red arrow) at any given azimuth angle θ measured from the North direction (y-axis), corresponds to the Q value for that azimuth. Azimuthal variations in Q are elliptical and the degree of anisotropy increases with offset. A minimum of 400 m is required to reveal the anisotropy. The major axis of the ellipse corresponds to fracture strike while the minor axis corresponds to the fracture normal

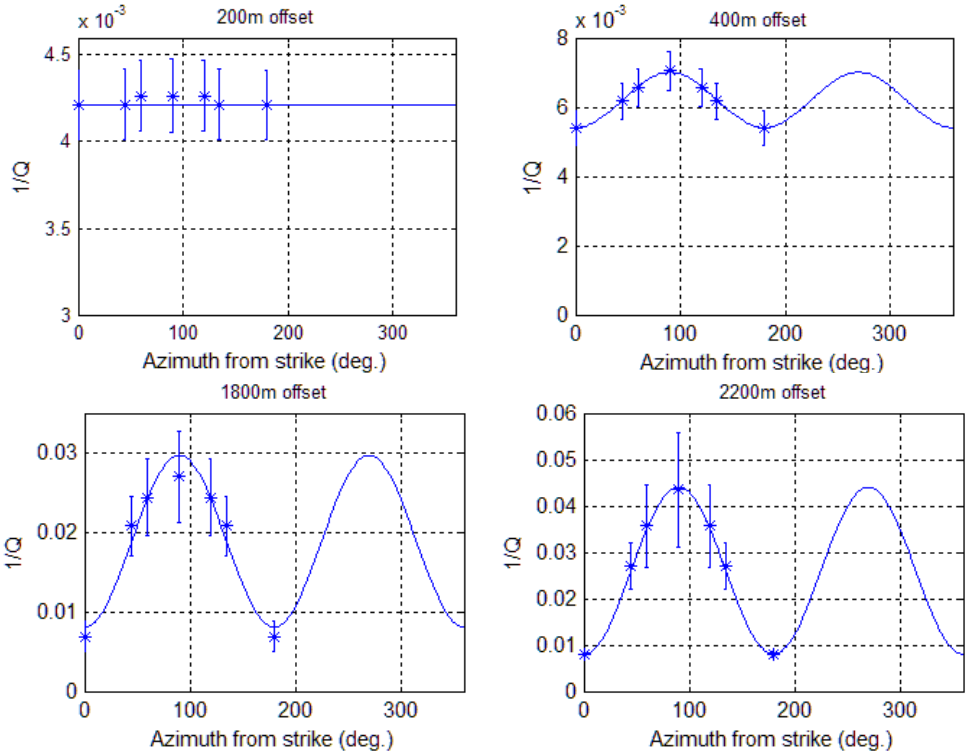

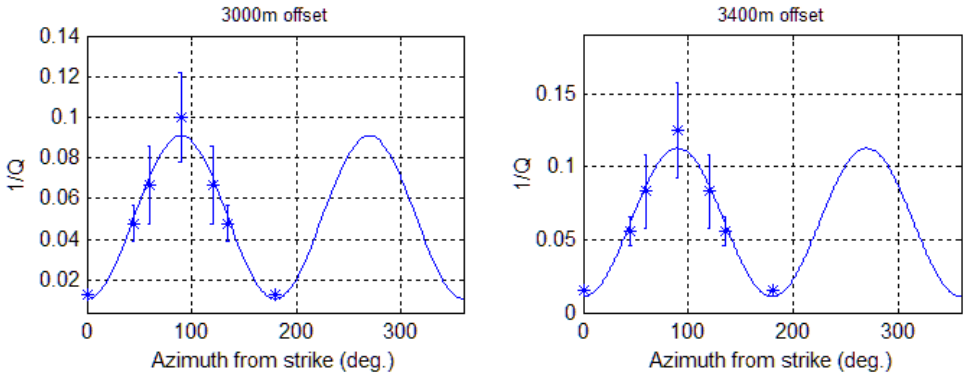

Figure 9: Cosine fits of estimated 1/Q values against azimuth for selected offsets. The degree of anisotropy increases with offset. No azimuthal variations are observed at 200 m offset (4.2° incidence angle). Maximum attenuation occurs 90° from the fracture strike direction.

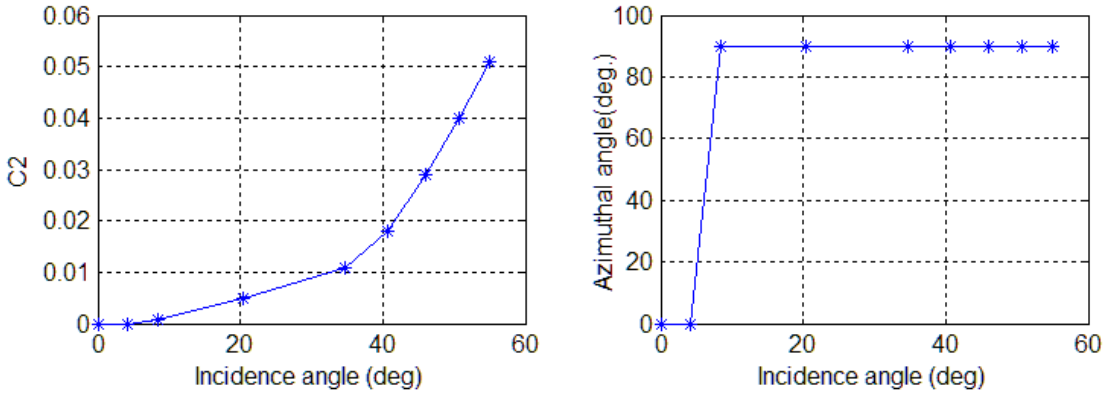

(a) (b)

Figure 10: Inverted parameter from cosine fits (a) C2. The degree of anisotropy increases with incidence angle. (b) Angle of minimum Q (maximum attenuation) - 90° from strike direction corresponding to fracture normal.

5.0 Conclusion

We have demonstrated that in fluid-saturated porous rocks, fluid mobility greatly influences seismic wave propagation, giving rise to systematic variations in attenuation as a function of material properties and the relative geometries of the recording array and the fractured medium. The relaxation time strongly controls the frequency range over which attenuation occurs.The induced attenuation increases with incidence (polar) angle and also away from the fracture strike direction, which is consistent with the seismic physical modelling studies of Ekanem *et al.* (2013) and the results of similar studies by Maultzsch *et al.* (2007) in a walk away VSP setting. Azimuthal variations in the induced attenuation are elliptical and the fracture orientations are quite easily obtained from the axes of the ellipse. Our findings thus, validate the current practice of using attenuation anisotropy as a potential tool to derive fracture properties from seismic data to supplement the use of amplitudes, travel time, velocity and AVO gradient attributes.

Acknowledgement

We are grateful to the Akwa Ibom State University (AKSU) - Nigeria for providing sponsorship to Ekanem's studies at the University of Edinburgh. We also thank all the sponsors of the Edinburgh Anisotropy Project (EAP) for supporting the project and the permission to publish the results.

References

Batzle, M. L.; Han, D-H and Hofmann, R., 2006. Fluid mobility and frequency dependent seismic velocity - Direct measurements. *Geophysics* **71**(1), N1 - N9.

Chapman M. 2003. Frequency-dependent anisotropy due to meso-scale fractures in the presence of equant porosity. *Geophysical Prospecting*, **51**, 369 - 379.

Chapman M., Maultzsch S., Liu E. and Li X.-Y. 2003. The effect of fluid saturation in an anisotropic multi-scale equant porosity model. *Journal of Applied Geophysics*, **54**, 191 - 202.

Clark, R.A., Benson, P.M., Carter, A.J and Guerrero Moreno, C.A., 2009. Anisotropic P-wave attenuation measured from a multi-azimuth surface seismic reflection survey. *Geophysical Prospecting*, **57**, 835 - 845.

Clark, R.A., Carter, A.J., Nevill, P.C. AND Benson, P.M., 2001. Attenuation measurement from surface seismic data - Azimuthal variation and time lapse case studies: *63rd Conference & Technical Exhibition*, *Expanded Abstracts*, EAGE, L-28.

Dasgupta, R. and Clark, R., 1998. Estimation of Q from surface seismic reflection data. Geophysics, **63**(6):2120 - 2128.

Ekanem, A. M., Wei, J., Li, X-Y., Chapman, M and Main, I. G., 2014. Effect of fracture aperture on P-wave attenuation: A seismic physical modelling study. *International Journal of Geophysics,* **2014,** ID 241279, 1-8.

Ekanem, A. M., Wei, J., Li, X. Y., Chapman, M and Main, I. G., 2013. P-wave attenuation anisotropy in fractured media: A seismic physical modelling study. *Geophysical prospecting,* **61**(suppl. 1), 420 - 433.

Eshelby, J.D., 1957. The determination of the elastic field of an ellipsoidal inclusion, and related problem. *Proceedings of the Loyal Society of London*, **A241**, 376 - 396.

Gardner, G. H. F., Wyllie, M. R. J. and Droschak, D. M., 1964. Effects of pressure and fluid saturation on the attenuation of elastic waves in sands. *Journal of petroleum Technology*, **16**, 189 - 198.

Hauge P.S. 1981. Measurements of attenuation from vertical seismic profiles. *Geophysics* **46**, 1548 -1558.

Johnston, D.H., 1981. Attenuation: A state of the art summary. Seismic Wave Attenuation, SEG geophysical reprint series, 123 - 135.

Johnston, D.H. and Toksöz, M.N., 1980. Ultrasonic P and S wave attenuation in dry and saturated rocks under pressure. *Journal of Geophysical Research*, **85**, 925 - 936.

Lucet, N. and Zinszner, B., 1992. Effects of heterogeneities and anisotropy on sonic and ultrasonic attenuation in rocks. *Geophysics*, **57**, 1018 - 1026.

Luo, M., Arihara, N., Wang, S., Di, B., and Wei, J., 2006. Abnormal transmission attenuation and its impact on seismic-fracture prediction – A physical modelling study. Geophysics, **71**, D15 - D22.

Maultzsch, S., Chapman, M. Liu, E. and X. Y. Li, 2007. Modelling and analysis of attenuation anisotropy in multi-azimuth VSP data from Clair field. Geophysical Prospecting, **55**, 627-642.

Maultzsch, S., M. Chapman, E. Liu, and X. Y. Li, 2003. Modelling frequency dependent seismic anisotropy in fluid-saturated rock with aligned fractures: Implication of fracture size estimation from anisotropic measurements. *Geophysical Prospecting*, **51**, 381 - 392.

Murphy, W.F., 1985. Sonic and ultrasonic velocities: Theory versus experiment. *Geophysical Research Letters*, **12**, 85 - 88.

Pujol J. and Smithson S. 1991. Seismic wave attenuation in volcanic rocks from VSP experiments. *Geophysics* **56**, 1441 - 1455.

Qian, Z.; Chapman, M; Li, X.Y; Dai, H.C.; Liu, E.; Zhang, Y.; and Wang, Y., 2007. Use of multi-component seismic data for oil-water discrimination in fractured reservoirs. *The Leading Edge*, **26**, 1176 - 1184.

Sothcott, J., McCann, C. and O'Hara, S., 2000. The influence of two pore fluids on the acoustic properties of reservoir sandstones at sonic and ultrasonic frequencies. *70th Ann. Internat. Mtg., Expanded Abstracts, Soc. of Expl. Geophys*, 1883 - 1886.

Taylor, D., 2001. ANISEIS v5.2 Manual. Applied Geophysical Software Inc., Houston.

Tod S.R. 2001. The effects on seismic waves of interconnected nearly aligned cracks. *Geophysical Journal International*, **146**, 249 - 263.

Toksõz, M. N., Johnston, D. H., and Timur, A., 1979. Attenuation of seismic waves in dry and saturated rocks: I. Laboratory measurements. *Geophysics*, **44**, 681 - 690.

Winkler, K.W., 1986. Estimates of velocity dispersion between seismic and ultrasonic frequencies. *Geophysics*, **51**, 183 - 189.